Published March 22, 2010

Myosin II activity regulates vinculin recruitment to focal adhesions through FAK-mediated paxillin phosphorylation

Ana M. Pasapera,[1] Ian C. Schneider,[3,4,7] Erin Rericha,[2,7] David D. Schlaepfer,[5,6] and Clare M. Waterman[1,7]

[1]Cell Biology and Physiology Center, National Heart, Lung, and Blood Institute, National Institutes of Health, Bethesda, MD 20892
[2]Institute for Research in Electronics and Applied Physics, University of Maryland, College Park, MD 20742
[3]Department of Chemical and Biological Engineering and [4]Department of Genetics, Development, and Cell Biology, Iowa State University, Ames, IA 50011
[5]Moores Cancer Center and [6]Department of Reproductive Medicine, University of California, San Diego, La Jolla, CA 92093
[7]Physiology Course, Marine Biological Laboratory, Woods Hole, MA 02543

Focal adhesions (FAs) are mechanosensitive adhesion and signaling complexes that grow and change composition in response to myosin II–mediated cytoskeletal tension in a process known as FA maturation. To understand tension-mediated FA maturation, we sought to identify proteins that are recruited to FAs in a myosin II–dependent manner and to examine the mechanism for their myosin II–sensitive FA association. We find that FA recruitment of both the cytoskeletal adapter protein vinculin and the tyrosine kinase FA kinase (FAK) are myosin II and extracellular matrix (ECM) stiffness dependent. Myosin II activity promotes FAK/Src-mediated phosphorylation of paxillin on tyrosines 31 and 118 and vinculin association with paxillin. We show that phosphomimic mutations of paxillin can specifically induce the recruitment of vinculin to adhesions independent of myosin II activity. These results reveal an important role for paxillin in adhesion mechanosensing via myosin II–mediated FAK phosphorylation of paxillin that promotes vinculin FA recruitment to reinforce the cytoskeletal ECM linkage and drive FA maturation.

Introduction

Cells impinge force on their extracellular environments during tissue morphogenesis, cardiovascular and pulmonary function, directed cell motility, and the immune response. Cell forces are primarily developed by myosin IIs acting in the actin cytoskeleton (Cai et al., 2006). Cytoskeletal forces are linked to the ECM through transmembrane α–β integrin heterodimers that cluster to form focal adhesions (FAs; Geiger et al., 2009). On their cytoplasmic face, integrin tails serve as scaffolds for the recruitment of FA-associated proteins, including cytoskeletal-binding and adapter proteins, and enzymes such as kinases, phosphatases, and small GTPases and their modulators (Zaidel-Bar et al., 2007a). These proteins contribute to FA functions in integrin-mediated signal transduction and form the force-bearing link between the ECM and cytoskeleton.

FAs are mechanosensitive organelles that recruit cytoplasmic proteins to grow and change composition in response to mechanical tension (Chrzanowska-Wodnicka and Burridge, 1996; Riveline et al., 2001) in a process known as FA maturation. Tension driving FA maturation can be supplied either by myosin II forces transmitted to FAs through the actin cytoskeleton or by external forces applied to the cell. It is thought that tension-driven FA compositional changes are critical to the ability of FAs to trigger different signaling pathways that promote differentiation, division, or apoptosis (Engler et al., 2006).

The mechanism of tension-mediated FA maturation is not well characterized. Tension on FA proteins could drive localized unfolding or conformational changes that unmask binding sites for cytoplasmic proteins (Vogel and Sheetz, 2006). For example, molecular dynamics simulations suggest that directional

Correspondence to Clare M. Waterman: watermancm@nhlbi.nih.gov

Abbreviations used in this paper: CB, cytoskeleton buffer; CCD, charge-coupled device; FA, focal adhesion; FAKi, FAK inhibitor; IP, immunoprecipitation; MEF, mouse embryonic fibroblast; PY, phosphotyrosine.

Supplemental Material can be found at:
http://jcb.rupress.org/content/suppl/2010/03/22/jcb.200906012.DC1.html

The Rockefeller University Press $30.00
J. Cell Biol. Vol. 188 No. 6 877–890
www.jcb.org/cgi/doi/10.1083/jcb.200906012

Published March 22, 2010

force on integrin cytoplasmic tails could induce separation of the α and β subunits (Zhu et al., 2008) to allow new protein binding. In vitro experiments suggest that forced unfolding of talin promotes vinculin binding (del Rio et al., 2009), whereas stretching p130cas unmasks a tyrosine substrate for Src family kinases (Sawada et al., 2006). However, whether these mechanisms operate in cells during physiological, myosin II–mediated FA maturation is not known.

In spite of the lack of mechanistic insight, it is well accepted that tension-mediated FA maturation involves a sequential cascade of compositional changes (Zaidel-Bar et al., 2004). FAs are initiated by activation of integrin extracellular heads' affinity for ECM through association of their cytoplasmic tails with the vinculin- and actin-binding protein talin (Tadokoro et al., 2003). Early after integrin activation, the adapter protein paxillin is recruited by an unknown mechanism, and more integrins cluster into FA (Laukaitis et al., 2001; Webb et al., 2004; Wiseman et al., 2004). Further FA growth is accompanied by the recruitment of the actin-bundling protein α-actinin (Choi et al., 2008), which with talin (Lee et al., 2004) may establish a link between integrins and the actin cytoskeleton. Myosin II is thought to transmit tension in an α-actinin–actin network to the integrin–ECM linkage. This tension promotes elongation of an adhesion-associated actin bundle where cytoskeletal adapter proteins vinculin and zyxin accumulate (Choi et al., 2008). In addition, tension on fibronectin-engaged β1 integrins promotes integrin head binding to secondary sites on fibronectin (Friedland et al., 2009), inducing recruitment and activation of the tyrosine kinase FAK (Shi and Boettiger, 2003; Friedland et al., 2009). Tyrosine phosphorylation of early FA proteins, including FAK, paxillin, and p130cas (Ballestrem et al., 2006), then act as scaffolds for phosphotyrosine (PY)-binding SH2 domain–containing proteins. There are also studies that show compositional differences between small or large FAs (Zaidel-Bar et al., 2003, 2007b; Zimerman et al., 2004), although the order of protein addition or the requirement for tension in their FA recruitment is not known.

To better understand tension-mediated FA maturation, we sought proteins that are recruited to FAs in a contractility-dependent manner and examined the mechanism for their myosin II–sensitive FA association. We find that FA localization of vinculin is myosin II and ECM stiffness dependent. By examining the effects of myosin II inhibition on protein interactions and phosphorylation, we deduce that the myosin II–dependent recruitment of vinculin to FA is mediated by FAK phosphorylation of paxillin, which creates binding sites in FAs for vinculin to drive FA maturation.

Results

Inhibition of myosin II activity affects adhesion morphology and alters cell migration

To gain insight into myosin II–mediated FA maturation, we characterized the effects of myosin II inhibition on migration and FA morphology in mouse embryonic fibroblasts (MEFs) adhered to coverslips coated with 5 µg/ml fibronectin.

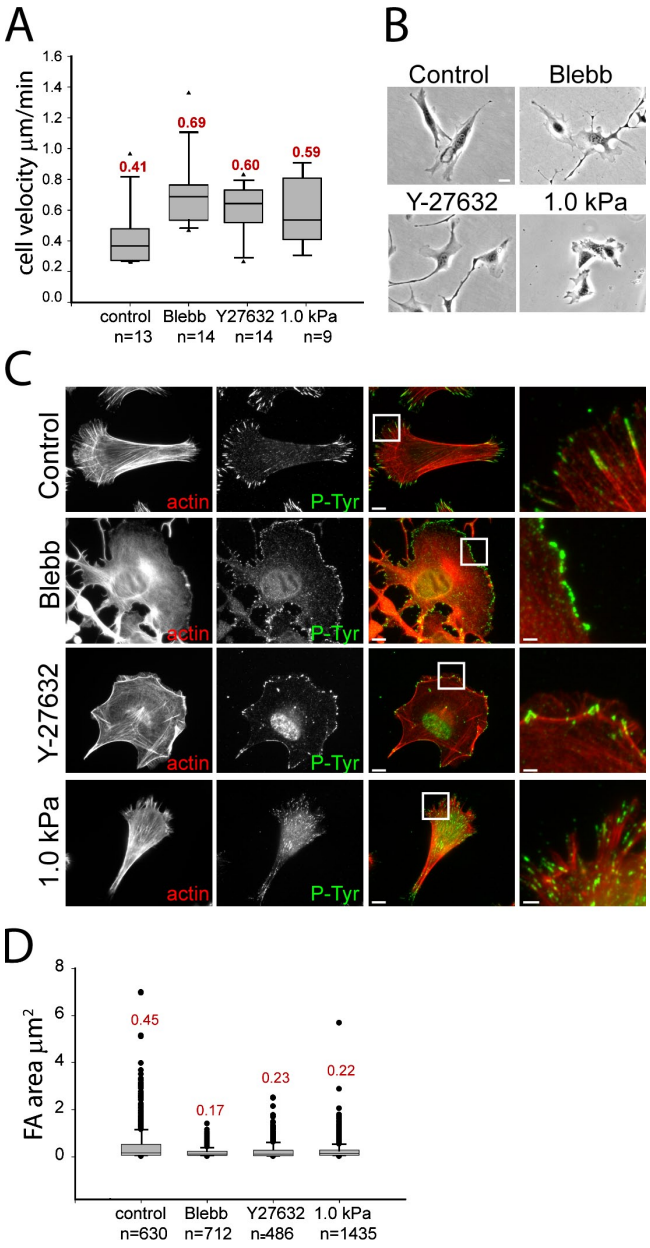

Figure 1. **Rho kinase–mediated myosin II activity and substrate stiffness slow MEF migration and increase adhesion size.** (A) Migration rates for untreated cells (control), cells treated with 20 µM blebbistatin (Blebb) or 10 µM Y27632, or plated on 1.0 kPa compliant polyacrylamide substrates. Mean velocity is shown above each box plot. Arrowheads indicate lower and upper extreme outliers. *n* = number of cells. (B) Phase-contrast images of cell morphology under the same conditions as in A. Bar, 10 µm. (C) Immunolocalization of PY epitopes (P-Tyr) to visualize adhesions (green) and fluorescent phalloidin staining to visualize actin filaments (red) under the treatments as in A. Merged images are shown in the third column, and boxed regions are magnified in the fourth column. Bars: (third column) 10 µm; (fourth column) 2 µm. (D) Area of individual adhesions within PY-immunolabeled cells under the conditions in A. Mean adhesion area (micrometer squared) is shown above each box plot. *n* = number of adhesions.

Contraction was inhibited with either 20 µM of the myosin II–specific ATPase inhibitor blebbistatin (K_i = 0.3 µM) or 10 µM of the Rho kinase inhibitor Y27632 (K_i = 0.14 µM). As a physiological approach to myosin II inhibition, MEFs were plated on fibronectin-coupled compliant substrates (1.0 kPa

Published March 22, 2010

polyacrylamide gel) where myosin II activity is down-regulated in response to mechanosensation of a compliant ECM (Pelham and Wang, 1997). Phalloidin staining and immunolocalization of PY epitopes (Thomas and Brugge, 1997) in control cells showed lamellipodia in the cell front and F-actin bundles in the center and tail, which often terminated in PY-containing FAs (Fig. 1 C). FAs ranged in size from diffraction limited (0.125 μm^2) at the cell front to several micrometers long (0.45 ± 0.75 μm^2) in the central and rear regions (Fig. 1 D). Because a goal of this study is to determine the compositional changes that accompany FA size changes mediated by myosin II, we will not classify different-sized structures as FAs, focal complexes, or fibrillar adhesions, but will refer to all membrane plaques marked by PY or another FA protein as adhesions. Blebbistatin treatment inhibited actin bundles and induced a homogeneous network, ROCK inhibition blocked central actin bundles, and plating on compliant substrates reduced actin bundle length and intensity compared with controls (Fig. 1 C). Myosin II inhibition by all three treatments decreased adhesion size compared with control (Fig. 1 D), and in the case of blebbistatin, confined adhesions to the extreme cell periphery (Fig. 1 C). These results agree with previous studies (Totsukawa et al., 2004; Even-Ram et al., 2007; Schaub et al., 2007). In addition, all three treatments altered cell morphology and increased migration rate compared with control (Fig. 1, A and B) as reported previously (Totsukawa et al., 2004; Even-Ram et al., 2007). Because myosin II ATPase and ROCK inhibition produced similar effects, in the remainder of our experiments, we used 20 µM blebbistatin (1 h) for pharmacological inhibition of myosin II, whereas compliant substrates were used for physiological down-regulation of contractility.

Adhesion recruitment of FAK, vinculin, zyxin, and α-actinin is myosin II dependent

To determine how adhesion composition is affected by actomyosin activity, we performed immunofluorescence and quantitative image analysis of cells in which contractility was inhibited. Because the adapter protein paxillin is a component of newly formed adhesions (Laukaitis et al., 2001; Choi et al., 2008), we examined the myosin II dependence of its localization to PY-containing adhesions. In both control and blebbistatin-treated cells, paxillin was nearly completely colocalized with PY in all adhesions in spite of blebbistatin's effects on adhesion size, spatial distribution, and actin organization (Fig. 2 A). Similarly, plating cells on compliant substrates did not alter localization of paxillin to PY-containing adhesions (Fig. S1). Thus, paxillin is present in adhesions independently of myosin II contractility, and therefore, we used it as an adhesion marker in further experiments.

We performed immunofluorescence and quantitative image analysis to examine the blebbistatin sensitivity of adhesion association of several important FA proteins. We determined the ratio of intensity of fluorescence in segmented adhesions in blebbistatin-treated cells relative to controls as a measure of the myosin II dependence of adhesion recruitment. This revealed a slight yet insignificant reduction in paxillin level after blebbistatin treatment in all experiments, ranging

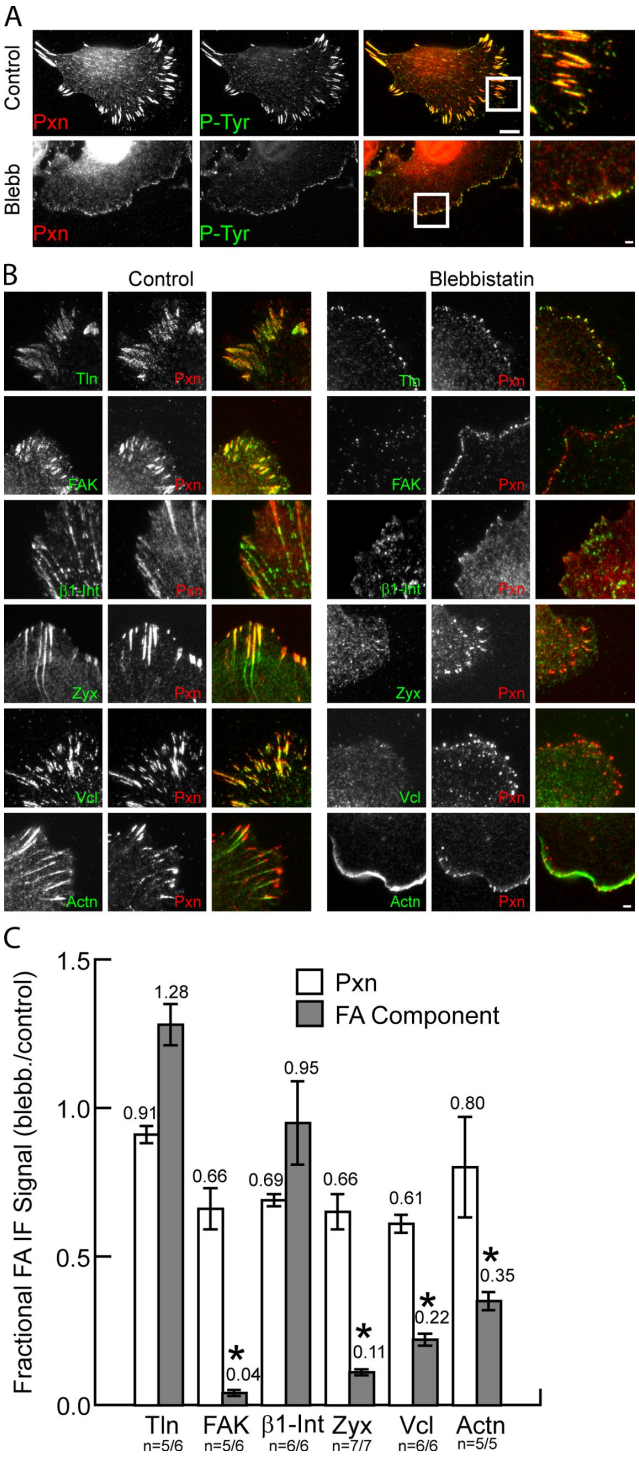

Figure 2. **Myosin II is required for recruitment of specific proteins to adhesions.** (A) Immunolocalization of paxillin (Pxn; red) and PY epitopes (P-Tyr; green) in untreated cells (control) or cells treated with 20 µM blebbistatin (Blebb). Merged images are shown in the third column, and boxed regions are magnified in the fourth column. Bars: (third column) 10 µm; (fourth column) 2 µm. (B) Immunolocalization of paxillin (red) with either (in green); talin 1 (Tln), FAK, β1 integrin (β1-Int), zyxin (Zyx), vinculin (Vcl), or α-actinin (Actn) in untreated control cells (left) or cells treated with 20 µM blebbistatin (right). Merged images are shown in the right column. Bar, 2 µm. (C) Effects of blebbistatin on adhesion localization of FA proteins expressed as the ratio of mean fluorescence intensities within segmented adhesions of blebbistatin-treated relative to control cells. Mean ratios are shown above each plot. *, $P < 0.02$. Error bars indicate 95% confidence interval of the mean. *n* = number of blebbistatin-treated cells/number of control cells.

Published March 22, 2010

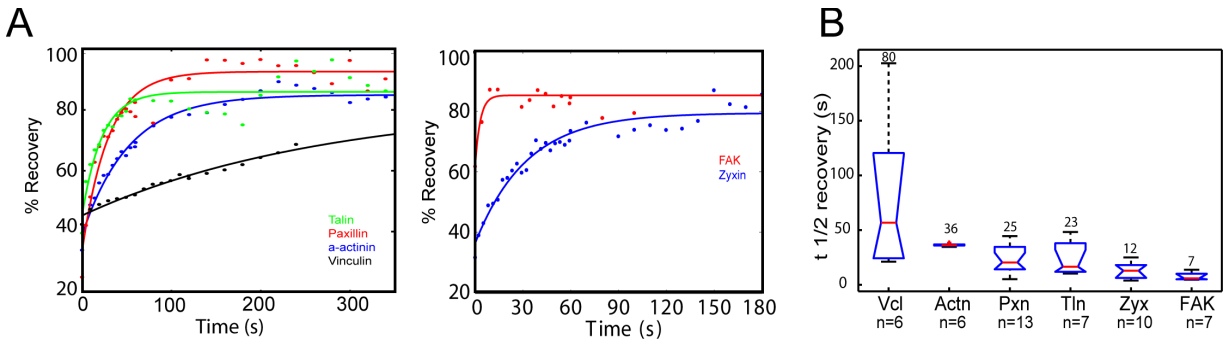

Figure 3. **Vinculin is stably bound in adhesions.** EGFP fusion proteins localized to adhesions were subjected to FRAP. (A) Sample fluorescence recovery curves for vinculin, α-actinin, talin 1, paxillin, FAK, and zyxin in single adhesions. Note different x-axis scales in left and right plots; fits are shown as solid lines. (B) Half-times of fluorescence recovery. Means are shown above each plot. Vcl, vinculin; Actn, α-actinin; Pxn, paxillin; Tln, talin 1; Zyx, zyxin. *n* = number of adhesions.

from 61 to 91% of controls (Fig. 2 C). Similar analysis revealed no significant difference in the levels of β1 integrin and talin in paxillin-containing adhesions between control and blebbistatin-treated cells (Fig. 2, B and C). In contrast, although there were high levels of FAK, zyxin, vinculin, and α–actinin in adhesions of controls, these proteins were significantly reduced in adhesions of blebbistatin-treated cells (Fig. 2 C). Blebbistatin caused redistribution of FAK, vinculin, and zyxin from adhesions to the cytosol, whereas α-actinin was relocalized to lamellipodia. (Fig. 2 B). Together, these results indicate that the recruitment of paxillin, talin, and β1 integrin to adhesions is independent of myosin II activity, whereas adhesion association of FAK, zyxin, vinculin, and α-actinin requires myosin II contraction.

Vinculin is a stably bound adhesion protein

We next hypothesized that strong adhesion binding affinity could override actomyosin dependence in recruitment of proteins to adhesions. To test this, we performed FRAP of EGFP-tagged proteins in single adhesions and determined the mean fluorescence recovery $t_{1/2}$ as an estimate of the stability of adhesion binding (Bulinski et al., 2001; Lele and Ingber, 2006). Our hypothesis predicts long FRAP $t_{1/2}$'s for the myosin II–independent adhesion-associated proteins paxillin and talin and short FRAP $t_{1/2}$'s for the blebbistatin-sensitive adhesion proteins zyxin, FAK, α-actinin, and vinculin. Contrary to our expectations, FRAP analysis revealed a broad range of mean $t_{1/2}$'s from <10 s to nearly 3 min with no correlation between myosin II dependence of adhesion association and FRAP $t_{1/2}$ (Fig. 3 and Fig. S2). EGFP conjugates of the myosin II–independent adhesion-associated proteins paxillin and talin had similar intermediate FRAP $t_{1/2}$'s of 23 ± 3.4 s (SEM) and 25 ± 5.9 s. The myosin II–dependent adhesion proteins exhibited FRAP $t_{1/2}$'s from very short, for EGFP-FAK (7 ± 2.1 s) and EGFP-zyxin (12 ± 2.5 s), to intermediate, for EGFP–α-actinin (36 ± 0.5 s), and to very long, for EGFP-vinculin (80 ± 2.9 s), which is longer than previous reports in other cell types (Chandrasekar et al., 2005; Möhl et al., 2009; Wolfenson et al., 2009). In addition, EGFP-vinculin often did not exhibit complete fluorescence recovery after 300 s (Möhl et al., 2009; unpublished data), suggesting the presence of a stably bound fraction in adhesions. Thus, different adhesion proteins possess highly variable adhesion-binding stability, which is independent of both protein class (i.e., adapter, kinase, and actin binding) and the myosin II dependence of their adhesion localization. Furthermore, in MEFs, the adapter protein vinculin exhibits particularly stable adhesion binding. Thus, we focused further study on the mechanism of actomyosin-dependent, stable vinculin association with adhesions.

Myosin II–mediated recruitment of vinculin to adhesions is cell type independent, reversible, and physiologically relevant

To characterize the generality of myosin II–dependent vinculin recruitment to adhesions, we examined its human cell type specificity. Immunofluorescence analysis of osteosarcoma (U2OS), breast epithelial (MCF-10), and endothelial (HUVEC) cell lines (Fig. S3) and primary foreskin fibroblasts (HFF-1; Fig. 4 A) revealed high levels of vinculin in adhesions of untreated cells but a significant reduction in vinculin in adhesions induced by blebbistatin treatment (Fig. 4 B).

To determine whether the blebbistatin-induced reduction of vinculin in adhesions was reversible, we analyzed the time course of vinculin recruitment after induction of actomyosin contractility by blebbistatin washout (Fig. 4, C and D). Immunofluorescence analysis showed that within 15 min after blebbistatin washout, although adhesion size was still reduced compared with controls, vinculin was already colocalized with paxillin in adhesions (Fig. 4, C and D). Analysis of later time points indicated that vinculin remained colocalized with paxillin, and normal adhesion size was regained within 30–60 min (Fig. 4, C and D). Thus, blebbistatin reversibly reduces vinculin in adhesions, and vinculin is recruited to adhesions soon after the induction of actomyosin contraction before the completion of adhesion growth.

We next sought to determine whether the myosin II–dependent recruitment of vinculin to adhesions occurs in physiologically relevant contexts. By examining vinculin localization in cells plated on compliant ECMs, we confirmed that reduction of contractility by ECM compliance mechanosensing reduced vinculin level in adhesions (Fig. S1). We next sought to determine when in the adhesion maturation cycle vinculin is recruited to adhesions of migrating cells. Similar to blebbistatin washout, in the advancing lamellipodium of migrating cells, nascent adhesions form independently of actomyosin contraction followed

Published March 22, 2010

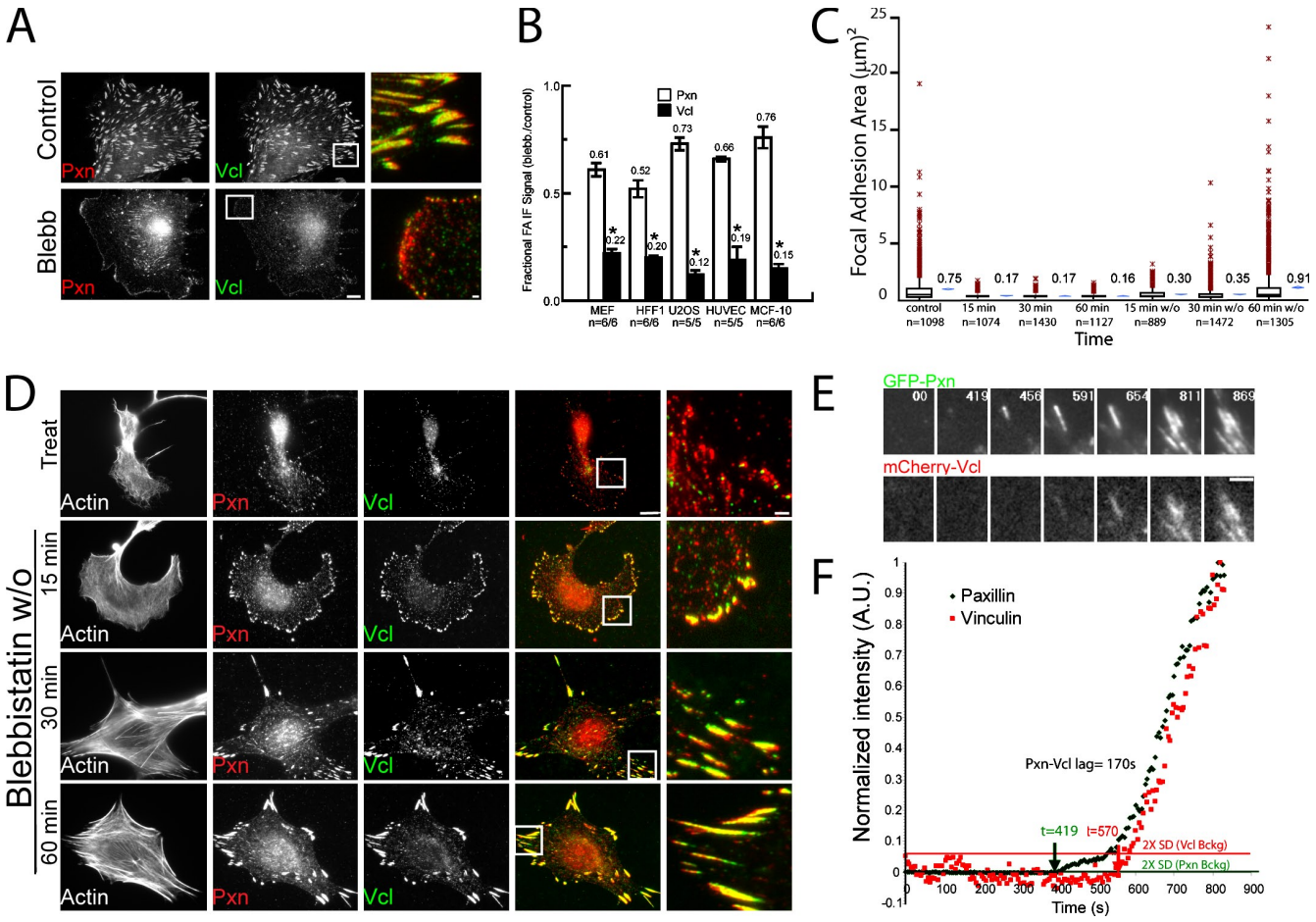

Figure 4. **Characterization of myosin II dependence of vinculin recruitment to adhesions.** (A) Immunolocalization in human foreskin fibroblasts (HFF1) of vinculin (Vcl; green) and paxillin (Pxn; red) in untreated (control) or 20 µM blebbistatin (Blebb)-treated cells. Bar, 10 µm. Merged, magnified images of boxed regions are shown in the third column. Bar, 2 µm. *n* = number of blebbistatin-treated cells/number of control cells. (B) Effects of blebbistatin on adhesion localization of paxillin and vinculin in the noted cell types expressed as the ratio of mean fluorescence intensities within segmented adhesions of blebbistatin-treated relative to control cells. Mean ratios are shown above each plot. *, $P < 0.02$. Error bars indicate 95% confidence interval of the mean. (C) Area of individual adhesions from paxillin immunostaining in MEF cells in untreated control cells at specific times after treatment with 20 µM blebbistatin (15, 30, and 60 min) or washout of 20 µM blebbistatin into control media (15, 30, and 60 min w/o). Mean adhesion areas (micrometer squared) are shown next to each box plot. Red symbols indicate the outliers at more than three interquartiles; blue symbols indicate a ~95% confidence interval of the mean. *n* = number of adhesions. (D) Immunolocalization of paxillin (red) and vinculin (green) and fluorescent phalloidin staining of actin filaments in cells after treatment (Treat) for 60 min and washout (blebbistatin w/o) for 15, 30, and 60 min of 20 µM blebbistatin. Merged images are shown in the fourth column, and boxed regions are magnified in the fifth column. Bars: (fourth column) 10 µm; (fifth column) 2 µm. (E) Images from a time-lapse dual-color TIRF series of EGFP-paxillin (GFP-Pxn) and mCherry vinculin (mCherry-Vcl) during adhesion formation and growth in a migrating MEF cell. Time is shown in seconds. Bar, 2 µm. (F) Normalized fluorescent protein intensity (green, paxillin; red, vinculin) in the adhesion shown in E. Horizontal lines show the value of two times the standard deviation of the normalized background fluorescence (2× SD Vcl or Pxn Bckg); note that this is higher for mCherry because it is much dimmer than EGFP. Arrows indicate the time when the intensity rose above these values. The time difference between arrows indicates lag time between the accumulation of EGFP-paxillin and mCherry-vinculin at the adhesion (Pxn-Vcl lag).

by their myosin II–dependent maturation (Riveline et al., 2001; Choi et al., 2008). MEFs were cotransfected with mApple- or EGFP-paxillin as a marker of nascent adhesions (Choi et al., 2008) and EGFP- or mCherry-vinculin and imaged by time-lapse TIRF microscopy (Fig. 4 E and Video 1). Quantitative analysis showed that the initiation of vinculin accumulation in adhesions lagged behind that of paxillin by 80 ± 40 s ($n = 16$ FAs in four cells; range 35–180 s; Fig. 4 F; Choi et al., 2008). The lag in vinculin accumulation relative to paxillin occurred independently of fluorescent tag or order of image acquisition (unpublished data). Together, these results suggest that the reversible, myosin II–dependent recruitment of vinculin to adhesions occurs in a range of cell types in the physiologically relevant contexts of ECM stiffness mechanosensing and adhesion maturation during cell migration.

The paxillin–vinculin interaction is modulated by myosin II activity

Our results show that the vinculin-binding proteins talin (Jones et al., 1989) and paxillin (Brown et al., 1996) are recruited to adhesions independent of myosin II, suggesting that they could serve as myosin II–sensitive scaffolds for recruitment of subsequent proteins. To determine whether vinculin interactions with talin or paxillin were altered by myosin II activity, we assayed their associations by immunoprecipitation (IP) from MEF lysates prepared in the presence or absence of

Published March 22, 2010

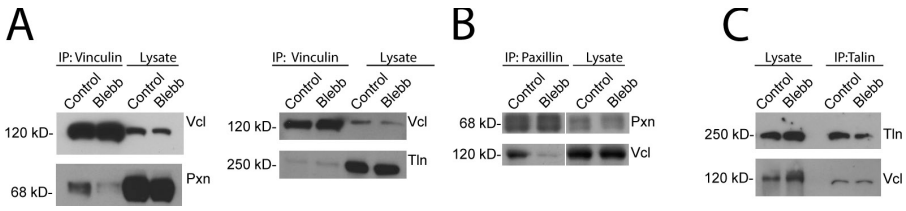

Figure 5. **Effects of myosin II inhibition on the interactions between vinculin, paxillin, and talin.** IPs were performed from lysates of untreated control MEFs (control) or MEFs treated with 20 µM blebbistatin (Blebb) followed by immunoblot analysis. (A) IP with anti-vinculin (Vcl) antibodies, immunoblot with anti-vinculin and antipaxillin (Pxn; left), or anti–talin 1 (Tln; right) antibodies. (B) IP with antipaxillin antibodies and immunoblotting with antivinculin antibodies. White lines indicate that intervening lanes have been spliced out. (C) IP with anti–talin 1 antibodies and immunoblotting with antivinculin antibodies are shown.

blebbistatin. IP with antivinculin antibodies followed by probing for coprecipitation of talin or paxillin revealed association of both talin and paxillin with vinculin in controls (Fig. 5 A). Surprisingly, the coprecipitation of paxillin with antivinculin antibodies was markedly reduced in lysates of blebbistatin-treated cells. Similarly, although vinculin was present in IPs performed with antipaxillin antibodies from controls, vinculin in paxillin IPs from blebbistatin-treated cells was substantially reduced (Fig. 5 B). In contrast, the level of talin in the vinculin IPs (or vinculin in talin IPs) was not changed by myosin II inhibition (Fig. 5, A and C) in spite of the reduction in vinculin but not of talin in adhesions of blebbistatin-treated cells, suggesting that these proteins form a complex in the cytoplasm. IP with a nonrelated antibody (anti-EGFP) did not coprecipitate vinculin (see Fig. 8 K), paxillin, or talin (not depicted). Therefore, in cell lysates, the paxillin–vinculin interaction is reduced by myosin II inhibition, whereas effects on talin–vinculin interaction are not detected. Thus, we focused further study on the role of paxillin in myosin II–mediated recruitment of vinculin to adhesions.

Myosin II activity promotes FAK-mediated paxillin phosphorylation

Because paxillin phosphorylation is critical to cell migration and adhesion maturation (Petit et al., 2000; Zaidel-Bar et al., 2003, 2007b; Webb et al., 2004; Nayal et al., 2006; Bertolucci et al., 2008), we examined its myosin II dependence. We first examined tyrosines 31 and 118 (pY31-paxillin and pY118-paxillin), whose phosphorylation mediates Crk interaction (Schaller and Parsons, 1995) yet also are close to the LD1 and LD2 domains that are in part responsible for FAK and vinculin binding (Brown et al., 1996). Immunoblotting cell lysates with phosphospecific antibodies showed that blebbistatin reduced the level of pY31- and pY118-paxillin to 45 and 24% of control (Fig. 6 A). In contrast, phosphorylation at serine 273, which is thought to mediate paxillin's interaction with the Rac1 regulatory complex of β-Pix, Pak, and Pkl/Git1 (Turner et al., 1999; Nayal et al., 2006; Schmalzigaug et al., 2007), was slightly enhanced to 127% of control by blebbistatin treatment (Fig. 6 D). Immunofluorescence and quantitative image analysis revealed a blebbistatin-induced slight reduction in pY31- and pY118-paxillin to 69% and 81% of that in control adhesions, respectively, similar to the blebbistatin-induced reduction in total paxillin in adhesions to 65–91% of controls (Fig. 2, B and C; and Fig. 6, B and C). These data, together with previous results (Zaidel-Bar et al., 2007b), suggest that contractility enhances paxillin phosphorylation on Y31/118.

To determine how myosin II–mediated effects on paxillin phosphorylation correlated with paxillin protein interactions, we performed paxillin IPs from lysates prepared in the presence and absence of blebbistatin and probed for interacting proteins. First, probing paxillin IPs with anti-PY antibodies showed that myosin II inhibition decreased the level of total paxillin PY (31%) by a similar amount as its reduction of pY31 and pY118 (Fig. 6 D) relative to controls. There was also a similar reduction to 12% and 66%, respectively, in the association of either FAK or Crk with paxillin in IPs from blebbistatin-treated cells compared with controls (Fig. 6 D). In contrast, myosin II inhibition increased the paxillin–β-Pix interaction to 159% of control (Fig. 6 D) and did not effect the adhesion localization of β-Pix (Fig. S4). Together, these results show that myosin II–dependent modulation of paxillin interactions correlates with its regulation of paxillin phosphorylation.

Integrin engagement promotes FAK recruitment to adhesions and activation by autophosphorylation on Y397 (pY397-FAK; Burridge et al., 1992; Shi and Boettiger, 2003). Thus, we examined the effects of myosin II activity on FAK Y397 phosphorylation. Immunoblotting of lysates revealed, similarly to ROCK inhibition in other cell types (Torsoni et al., 2005), that blebbistatin treatment or plating cells on compliant substrates substantially reduced pY397-FAK relative to control (Fig. 6 G and Fig. S1). Immunofluorescence showed a blebbistatin-induced reduction in pY397-FAK that mirrored the reduction of total FAK in adhesions (Fig. 2, B and C; Fig. 6, E and F; and Fig. S1). In contrast, the activity of Src, another kinase known to act with FAK on paxillin Y31/118 (Turner, 2000), was not affected by blebbistatin treatment, as assayed by immunoblotting for dephosphorylation on Src Y527 (Fig. 6 G; Kmiecik and Shalloway, 1987). Thus, full FAK adhesion association and activation requires myosin II contractility.

Because phosphorylation of Y31/118 on paxillin is regulated by FAK (Bellis et al., 1995; Schaller and Parsons, 1995), our results suggest that the blebbistatin-induced effects on paxillin phosphorylation could be mediated through FAK. Indeed, by immunoblotting cell lysates, we found that paxillin phosphorylation was at similar levels in lysates of cells treated with blebbistatin, 10 µM of a small molecule FAK inhibitor (FAKi; PF271; Roberts et al., 2008), or both (Fig. 6 G and Fig. S5 A). In addition, inhibition of Src by PP2 treatment did not further decrease the paxillin phosphorylation by blebbistatin but curiously

Published March 22, 2010

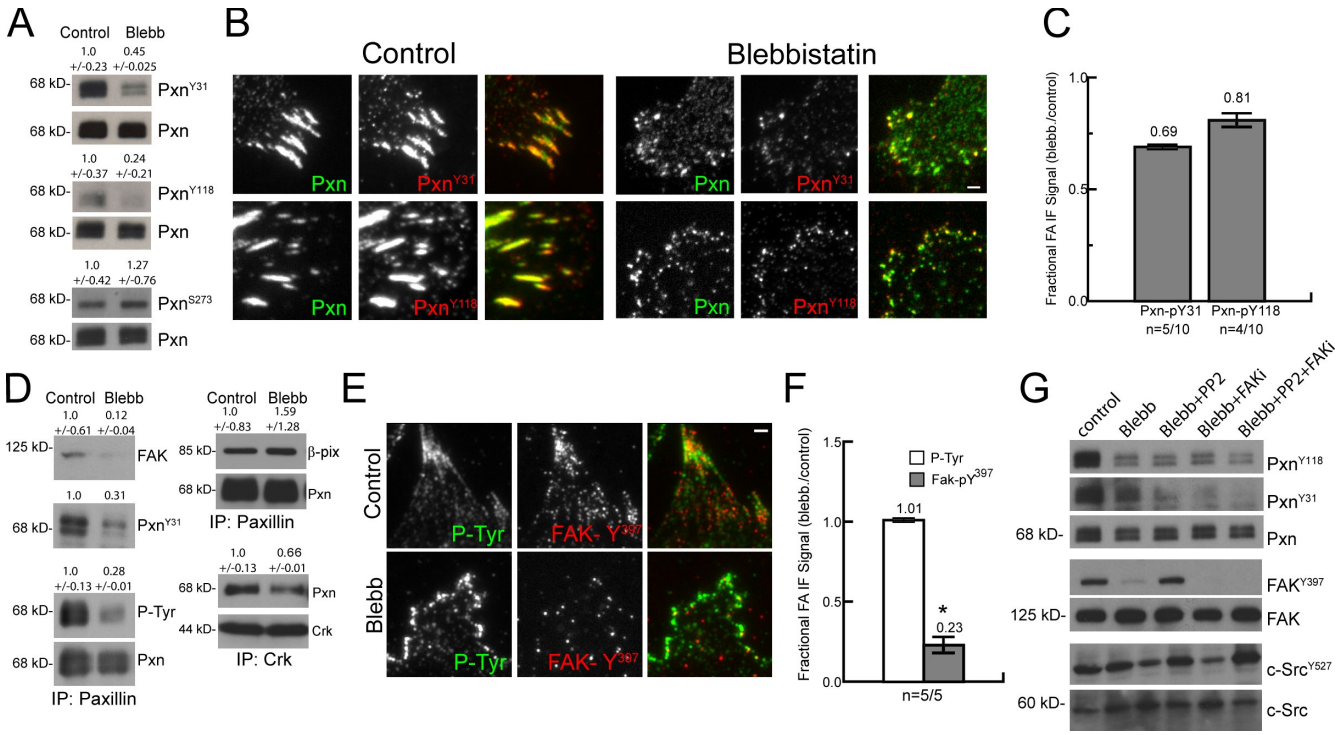

Figure 6. **Myosin II promotes tyrosine phosphorylation and interaction of paxillin, vinculin, and FAK.** (A) Immunoblot of lysates of untreated MEF cells (control) and cells treated with 20 µM blebbistatin (Blebb) using antibodies specific to paxillin (Pxn) or pY31, pY118, or pS273 paxillin (Pxn^{Y31}, Pxn^{Y118}, and Pxn^{S273}). Numbers above each blot represent the mean of quantified Western blots ± 95% confidence interval (n = 4 experiments). (B) Immunolocalization of paxillin (green) and pY31 or pY118 paxillin (red) in untreated control cells and cells treated with 20 µM blebbistatin. The third columns show merged images Bar, 2 µm. (C) Effects of blebbistatin on adhesion localization of pY31 and pY118 paxillin in adhesions, expressed (also in F) as the ratio of mean fluorescence intensities within segmented adhesions of 20 µM blebbistatin-treated relative to control cells. Antibody competition for similar epitopes precluded comparison with effects of blebbistatin on total paxillin level in the same cells. Mean fluorescence ratio is shown above each plot. n = number of blebbistatin-treated cells/number of control cells (also in F). (D) IP with antibodies to paxillin (left and top right) or Crk (bottom right) from lysates of untreated control MEFs or MEFs treated with 20 µM blebbistatin followed by immunoblotting with antibodies to paxillin, PY epitopes (P-Tyr), pY31 paxillin, FAK, β-Pix, or Crk. Numbers above each blot represent the mean of quantified Western blots ± 95% confidence interval (n = 3 experiments). (E) Immunofluorescence analysis of untreated control cells or cells treated with 20 µM blebbistatin using antibodies specific to pY397 FAK (red) or PY epitopes (green). Merged images are shown in the third column. Bar, 2 µm. (F) Effects of 20 µM blebbistatin on adhesion localization of pY397 FAK and PY in adhesions quantified from immunofluorescence images. *, $P < 0.02$. (G) Immunoblot of lysates of untreated MEF cells, cells treated with 20 µM blebbistatin, or a combination of 20 µM blebbistatin and either 10 µm PP2, 10 µm PF271 (FAKi), or all three using antibodies specific to paxillin, pY31, pY118 paxillin, FAK, pY397 FAK, Src (c-Src), or pY527 Src ($cSrc^{Y527}$). Error bars indicate 95% confidence interval of the mean.

restored some blebbistatin-induced FAK inactivation (Fig. 6 G). Together, these data suggest that myosin II–dependent recruitment and activation of FAK at adhesions mediates phosphorylation of paxillin on Y31/118.

Paxillin Y31/118 phosphomimic is sufficient to promote paxillin–vinculin interaction and vinculin recruitment to adhesions

We next sought to determine the requirement for paxillin and its regulation by phosphorylation in the recruitment of vinculin to adhesions. Unfortunately, because cells lacking talin have no adhesions (Zhang et al., 2008), talin's role in vinculin adhesion recruitment cannot be determined. In contrast, the requirement for paxillin in vinculin adhesion recruitment is controversial because vinculin is present in adhesions of embryonic stem cells lacking the paxillin gene (Hagel et al., 2002), whereas in smooth muscle cells, vinculin recruitment to the membrane requires paxillin (Opazo Saez et al., 2004). However, cells in these previous studies, as well our MEFs (Fig. 7 A), likely express the closely related paxillin homologue Hic-5 that also binds vinculin (Thomas et al., 1999). Therefore, we performed knockdowns of paxillin and/or Hic5 by siRNA and assayed for the presence of vinculin in adhesions. 48 h after transfection of MEFs with oligonucleotide pools, the levels of paxillin and Hic-5 protein were reduced by 45% and 75%, respectively, with even lower levels in the double knockdown (75% for both paxillin and Hic5; Fig. 7 A). Immunofluorescence revealed that cells with reduced levels of either paxillin, Hic5, or both were small and poorly spread (Fig. 7 B). Double-depleted cells displayed marked reduction in talin or PY-containing adhesions except in cell regions containing residual clustered paxillin/Hic5 (Fig. 7 C). Instead, talin in depleted cells was evenly distributed in dim, diffraction-limited punctae, PY staining was reduced, and interference reflection microscopy confirmed the absence of localized areas of close contact with the substrate in paxillin/Hic5-depleted cells (unpublished data). Immunolocalization of vinculin revealed a similar localization as talin in the double-depleted cells (Fig. 7 C). In addition, we were unable to find cells completely lacking

Published March 22, 2010

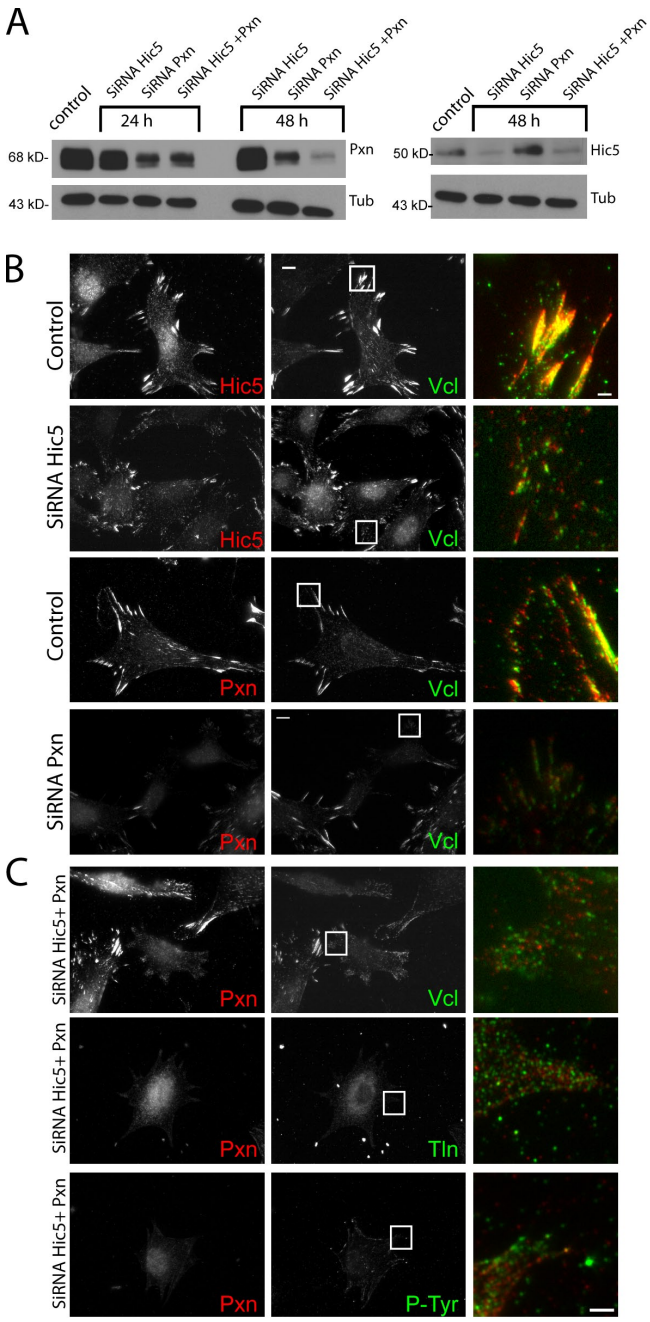

Figure 7. **Requirement for paxillin and Hic5 for adhesion formation.** (A) Immunoblot analysis of paxillin (Pxn; left), Hic5 (right), and tubulin (Tub; both) in lysates of mock-transfected cells or cells transfected with siRNA pools against paxillin, Hic5, or both. (B) Immunofluorescence localization of Hic5 (red), paxillin (red), and vinculin (Vcl; green) in control cells or cells transfected with siRNA pools against paxillin or Hic5. (C) Immunofluorescence localization of paxillin (red) and vinculin, talin 1 (Tln), or PY epitopes (P-Tyr; green) in control cells or cells transfected with siRNA pools against both paxillin and Hic5. (B and C) Merged images of boxed regions are magnified in third columns. Bars, 2 µm.

paxillin or Hic5, and no changes in adhesions were seen after treatment with scrambled siRNA controls (unpublished data). These results suggest that paxillin and/or Hic5 are necessary for formation of discrete substrate adhesions, which precludes our ability to determine the requirement for these proteins in vinculin recruitment to adhesions.

We next sought to determine the requirement for paxillin phosphorylation in vinculin recruitment to adhesions. To determine whether enhanced phosphorylation could induce vinculin recruitment to adhesions in the absence of contractility, we promoted tyrosine phosphorylation in blebbistatin-treated cells by inhibition of tyrosine phosphatases with 100 µM sodium orthovanadate (Na_3VO_4) or 10 µM phenylarsine oxide (unpublished data). Phosphatase inhibition reversed the blebbistatin-induced decrease in pY31-paxillin and pY397-FAK (Fig. 8 A). In addition, IP and immunofluorescence analysis revealed that Na_3VO_4 treatment rescued the blebbistatin-induced reduction in vinculin–paxillin coprecipitation and vinculin localization in adhesions, although it did not rescue other effects of blebbistatin, including reduction in adhesion size and loss of central adhesions (Fig. 8, B–D).

To determine whether paxillin phosphorylation was sufficient to promote vinculin recruitment to adhesions or whether additional myosin II–dependent processes were required, we overexpressed EGFP-tagged paxillin mutants that were either unphosphorylatable (Y31/118F) or that mimicked phosphorylation charges (Y31/118E) at Y31/118 (Zaidel-Bar et al., 2007b) and examined their effects on the blebbistatin sensitivity of vinculin localization to adhesions. This revealed colocalization of both EGFP-tagged paxillin mutants with vinculin at adhesions of control cells (Fig. 8 E), with Y31/118F EGFP-paxillin inducing larger adhesions and the Y31/118E mutant inducing smaller adhesions (Zaidel-Bar et al., 2007b). Vinculin localizing in Y31/118F EGFP-paxillin–containing adhesions suggests either a parallel pathway for vinculin recruitment (e.g., talin) or the effects of endogenous paxillin. Importantly, expression of the Y31/118E EGFP-paxillin mutant rescued the blebbistatin-induced reduction of vinculin but not zyxin or α-actinin in small, peripheral adhesions (compare Fig. 8, E–H; with Fig. 2, B and C). FRAP analysis of mCherry vinculin in adhesions of cells expressing wild-type or Y31/118E EGFP-paxillin revealed long $t_{1/2}$'s of fluorescence recovery (Fig. 8 I). In contrast, mCherry vinculin in adhesions of blebbistatin-treated cells expressing Y31/118E EGFP-paxillin displayed a significant reduction in FRAP $t_{1/2}$ (Fig. 8 I), indicating a labile vinculin–adhesion association. In contrast, neither the Y31/118F EGFP-paxillin mutant nor vinculin localized to PY-containing adhesions in blebbistatin-treated cells (Fig. 8 E). Corroborating the results of immunofluorescence, IP from lysates of blebbistatin-treated cells using anti-GFP antibodies showed increased coprecipitation of vinculin with EGFP-tagged Y31/118E paxillin compared with EGFP-tagged wild-type or Y31/118F paxillin (Fig. 8 K). Expression of both mutant and wild-type EGFP-tagged paxillins reduced the level of endogenous paxillin phosphorylation in both untreated and blebbistatin-treated cells by similar amounts, possibly by competition between endogenous and expressed proteins for cellular kinases (Fig. 8 J). Expression of EGFP conjugates of any of the single paxillin tyrosine mutants (Y31E, Y31F, Y118E, and Y118F) gave partial effects compared with the double mutants in both immunofluorescence and IP assays (unpublished data). Together, these results suggest that paxillin Y31/Y118 phosphorylation is sufficient for promoting the

Published March 22, 2010

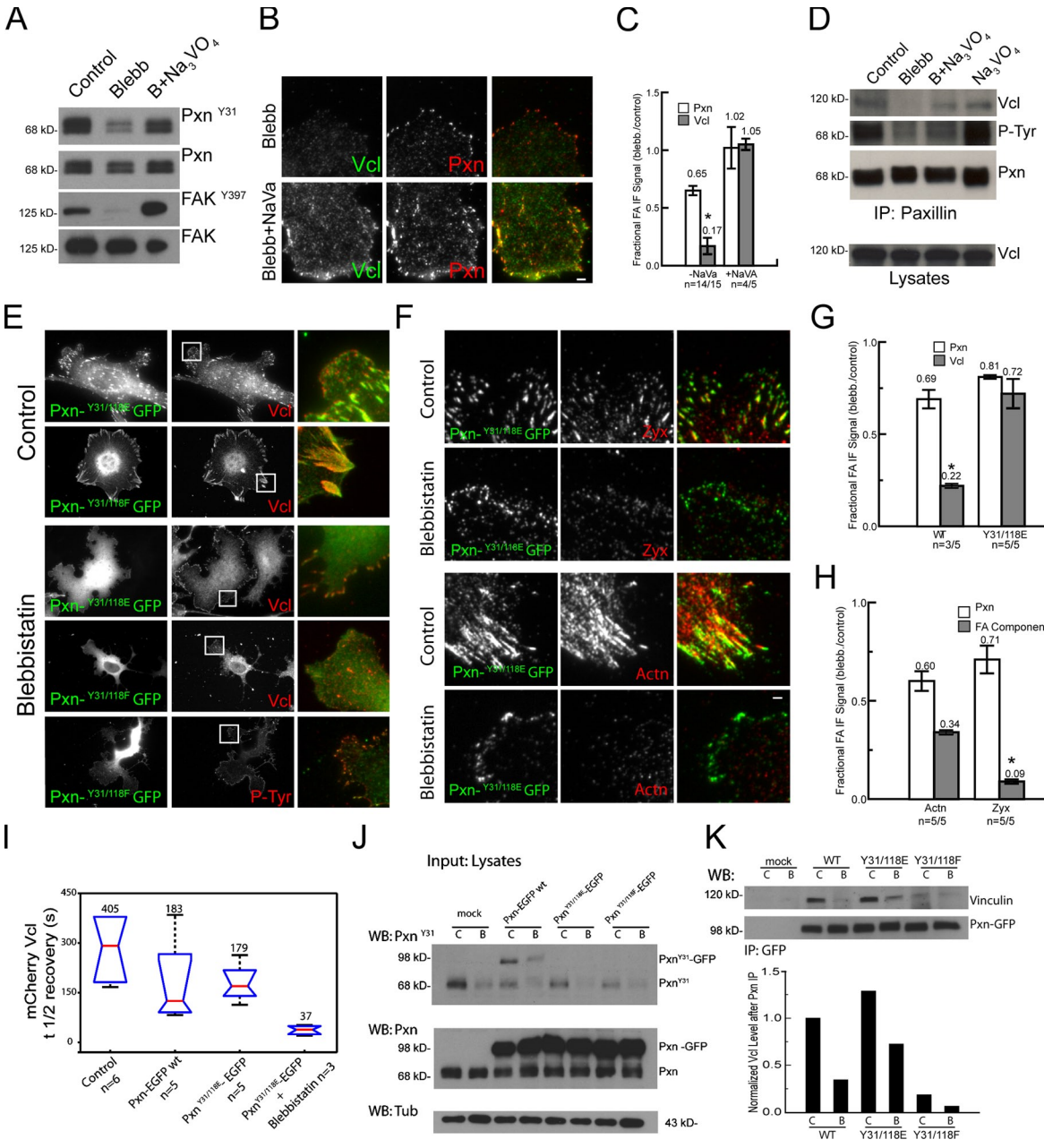

Figure 8. **Paxillin Y31/118 phosphorylation is sufficient for promoting paxillin–vinculin interaction and labile vinculin recruitment to adhesions.** (A) Immunoblot analysis of lysates of untreated (control) and cells treated with 20 µM blebbistatin (Blebb) or with 20 µM blebbistatin and 100 µM Na_3VO_4 using antibodies specific to paxillin (Pxn), pY31 paxillin, pY397FAK, or FAK. (B) Comparison of cells treated with 20 µM blebbistatin or 20 µM blebbistatin and 100 µM Na_3VO_4 and immunolabeled with antibodies to paxillin (red) and vinculin (Vcl; green). Bar, 2 µm. (C) Effects of Na_3VO_4 on vinculin localization in adhesions of blebbistatin-treated cells, shown (also in G and H) as the ratio of mean fluorescence intensities within segmented adhesions of 20 µM blebbistatin-treated cells relative to non–blebbistatin-treated cells in the presence and absence of additional Na_3VO_4. The mean fluorescence ratio is shown above each plot. (D) Antipaxillin IPs from lysates of untreated control or cells treated with either 20 µM blebbistatin, 100 µM Na_3VO_4, and 20 µM blebbistatin or 100 µM Na_3VO_4 alone followed by analysis by PAGE and immunoblotting with antibodies to vinculin, paxillin, or PY epitopes. (E–I) EGFP-conjugated paxillin (Pxn-GFP wt) or paxillin bearing mutations of tyrosines 31 and 118 to phenylalanines (Pxn Y31/118F) or glutamic acids (Pxn Y31/118E) were expressed in MEFs and either treated with 20 µM blebbistatin or not. (E) Images of cells expressing EGFP-conjugated paxillin mutants (green) and immunolocalization of vinculin (red) or PY epitopes (P-Tyr; red). Right columns show (also in F) merged, magnified images of the boxed regions Bar, 2 µm. (F) Images of EGFP-conjugated Y31/118E paxillin (green) and immunolocalization of zyxin (Zyx; red) or α-actinin (Actn; red) in cells treated with 20 µM blebbistatin. (G) Effects of blebbistatin on adhesion localization of vinculin and paxillin in cells overexpressing wild type (WT) or mutant (Y31/118E) paxillin-EGFP. (H) Effects of blebbistatin on adhesion localization of zyxin, α-actinin, and paxillin in cells overexpressing Y31/118E paxillin-EGFP. (I) FRAP analysis of mCherry-vinculin. mCherry-vinculin was expressed alone (control) or together with EGFP conjugates of wild-type or Y31/118E paxillin in untreated cells or cells treated with 20 µM blebbistatin (+Blebb), and FRAP was performed of the mCherry vinculin fraction in adhesions. Half-times of mCherry vinculin fluorescence recovery. Means are shown above each plot. *n* = number of adhesions. (J) Immunoblots of lysates of blebbistatin-treated (B) or untreated (C) cells that had been mock transfected or transfected with the EGFP-paxillin mutants and probed with antibodies to paxillin, pY31 paxillin, or tubulin. (K) Anti-GFP immunoprecipitates from MEFs expressing EGFP-tagged paxillins and either untreated (C) or treated with 20 µM blebbistatin (B) and probed by immunoblotting with antibodies to vinculin and GFP. Quantification of blots is shown below. WB, Western blot. *, $P < 0.02$. Error bars indicate 95% confidence interval of the mean. (C, G, and H) *n* = number of blebbistatin-treated cells/number of control cells.

Published March 22, 2010

paxillin–vinculin interaction and induction of a specific, labile association of vinculin with immature adhesions independent of myosin II activity.

Because our results showed that FAK is critical for Y31/118 paxillin phosphorylation, we finally sought to determine whether FAK activation is necessary or sufficient to induce the vinculin–paxillin interaction or vinculin recruitment to adhesions independent of myosin II activity. Unfortunately, this was difficult to assess because constitutively active FAK (Δ1–100 FAK) does not target to adhesions and causes cell rounding (Schlaepfer and Hunter, 1996), whereas inhibition of FAK affects adhesion turnover (Ilić et al., 1995; Webb et al., 2004). Indeed, treatment of cells with FAKi did not alter coprecipitation of vinculin with paxillin or recruitment of vinculin to paxillin-containing adhesions (Fig. S5). This is not surprising because inhibition of FAK or myosin II induces opposite adhesion phenotypes: FAK inhibition causes long-lived large adhesions (Fig. S5; Ilić et al., 1995), whereas myosin II inhibition promotes rapid turnover of tiny adhesions (Fig. 1; Webb et al., 2004; Choi et al., 2008). Thus, although the myosin II–dependent vinculin–paxillin interaction correlates with phosphorylation of FAK-regulated sites on paxillin, there are additional FAK-independent pathways to recruit vinculin to large and stable adhesions in the presence of cellular contractility.

Discussion

Our study has uncovered an important physiological role in adhesion maturation for paxillin in its interaction with the cytoskeletal adapter protein vinculin. To understand tension-mediated FA maturation, we sought proteins recruited to FAs in a myosin II–dependent manner and examined the mechanism of their myosin II–sensitive FA association. Using pharmacological inhibition of myosin II and ECM compliance to modulate cellular tension, we show that paxillin, talin, and β1 integrin recruitment to adhesions is independent of myosin II activity, whereas adhesion association of FAK, zyxin, α-actinin, and vinculin is promoted by myosin II contraction. We focused on the myosin II–dependent recruitment of vinculin to adhesions, showing that it is reversible and occurs across a range of cell types and in the physiologically relevant contexts of myosin II–induced adhesion maturation during cell migration and ECM stiffness mechanosensing. Although previous studies correlated vinculin accumulation to sites of applied tension on cells (Galbraith et al., 2002; Möhl et al., 2009), we show the first demonstration of myosin II–dependent vinculin adhesion association. By assessing the myosin II sensitivity of vinculin's protein interactions in cell lysates, we show that the vinculin–paxillin interaction is promoted by signaling induced by myosin II contractility, whereas we did not detect myosin II–dependent changes in the vinculin–talin interaction. It was recently shown that stretching talin promotes increased vinculin binding in vitro (del Rio et al., 2009). The IPs used in our study bias detection of myosin-dependent changes that are preserved in cell lysates, such as covalent phosphorylation of paxillin, whereas cell lysis would clearly disrupt stretch activation of talin. However, our results suggest that paxillin may be a critical protein, possibly in addition to talin, in the myosin II–dependent recruitment of vinculin to adhesions in cells.

This study also reveals a currently unknown role for paxillin phosphorylation in regulation of its interaction with vinculin in cells. We found that that in addition to vinculin, paxillin's interactions with FAK and Crk are promoted by myosin II activity, protein interactions specific to regulation by paxillinY31/118 phosphorylation (Turner, 2000). This suggests the interesting possibility that Crk signaling through paxillin to regulate transcription may be mechanosensitive. We also found that myosin II activity promotes phosphorylation of an activating tyrosine on FAK, which mediates the myosin II–dependent phosphorylation of paxillin on Y31 and Y118. Although reduction of contractility did not completely abrogate paxillin phosphorylation in adhesions, the phosphorylation of these residues is sufficient to promote paxillin-mediated recruitment of vinculin because phosphatase inhibition or overexpression of a phosphomimic promoted the paxillin–vinculin interaction and vinculin recruitment to adhesions independent of myosin II activity. We suggest that in nascent, low contractility adhesions, paxillin phosphorylation may be below a threshold required to accumulate substantial vinculin, with its labile binding to these sites as shown by FRAP (Fig. 8 I). As actomyosin contractility begins to mature adhesions, the increased FAK activity it promotes may amplify paxillin phosphorylation to the point that even low affinity vinculin binding is sufficient for visible adhesion accumulation.

Our results, together with those of others, support a speculative two-step "hand-off" model for myosin II–mediated vinculin adhesion recruitment and its role in adhesion maturation. We suggest that nascent adhesions form by myosin II–independent talin recruitment to and activation of β1 integrin (Fig. 2; Tadokoro et al., 2003), which together with talin's actin-binding activity (Jones et al., 1989) may promote formation of initial ECM–integrin–talin–actin linkages (Jiang et al., 2003). Paxillin is also recruited to nascent, myosin II–independent adhesions by an unknown mechanism (Fig. 2; Webb et al., 2004; Choi et al., 2008), and paxillin/Hic5 and talin are all required for formation of adhesion clusters (Fig. 7; Zhang et al., 2008). Myosin II activity in an α-actinin cross-linked cytoskeleton (Choi et al., 2008) generates tension that is transmitted to nascent adhesions. Tension across the ECM–integrin–talin–actin linkage promotes engagement of secondary binding sites between β1 integrin and fibronectin to induce recruitment and activation of FAK (Friedland et al., 2009), which is coupled to FAK/Src-dependent phosphorylation of paxillin Y31/118 (Fig. 6; Zaidel-Bar et al., 2007b). pY31/118 paxillin, with its newly revealed vinculin-binding site (Fig. 5), may cycle between adhesion-bound and cytosolic fractions, inducing labile vinculin recruitment to adhesions (Fig. 8). Subsequent to adhesion recruitment, activation of vinculin's actin-binding activity by simultaneous proximity to talin, actin, and acidic phospholipids (Chen et al., 2006) induces activation and hand off of vinculin from labile paxillin binding to these other partners, enhancing vinculin's binding stability to adhesions (Figs. 3 and 8) and reinforcing the cytoskeleton–ECM

Published March 22, 2010

linkage. The now matured adhesion can transmit stronger forces (Galbraith et al., 2002) to promote adhesion turnover in cell migration (Webb et al., 2004; Zaidel-Bar et al., 2007b). High forces across the cytoskeleton–integrin link may induce a parallel pathway for vinculin recruitment by stretch activation of vinculin-binding sites in talin (del Rio et al., 2009).

Questions remain about the paxillin-mediated recruitment of vinculin to adhesions. Because vinculin does not contain PY-binding SH2 domains, it is not clear how paxillin phosphorylation induces its interaction with vinculin or whether this interaction is direct. pY31/Y118 could induce a conformational change in paxillin that unmasks adjacent LD1 and LD2 domains involved in vinculin binding (Bertolucci et al., 2008). Additionally, the alternate pathways for vinculin adhesion recruitment that occur when FAK is inhibited (Fig. S5) remain unknown. Future studies may help to clarify these and other questions.

Materials and methods

Cell culture, transfection, and reagents

MEFs were obtained from American Type Culture Collection and maintained in DME supplemented with 10% FBS (Invitrogen) at 5% CO_2. For experiments, cells were plated on 22 × 22–mm #1.5 coverslips that had been coated with 5 µg/ml fibronectin (EMD) in PBS for 2 h at 37°C. Cells were plated at a low confluency (30–40%) for 16 h before experimental manipulations. Cells were transfected by nucleofector (Lonza) by using MEF1 solution and program T20. The following pharmacological inhibitors were used: 20 µM blebbistatin (Toronto Research Chemicals), 10 µM Y-27632 ROCK inhibitor (EMD), 10 µM Src inhibitor PP2 (EMD), 100 µM FAKi PF-271 (Roberts et al., 2008), 100 µM Na_3VO_4 (Sigma-Aldrich), and 10 µM phenylarsine oxide (Sigma-Aldrich). The following antibodies were used: rabbit anti–pY118-paxillin, rabbit anti–pY31-paxillin, rabbit anti–pY397-FAK, mouse anti-FAK, and rabbit anti–pY273-paxillin (Invitrogen); mouse anti-Hic5, mouse antipaxillin, and mouse anti-Crk (BD); rabbit antipaxillin (Santa Cruz Biotechnology, Inc.); mouse antitalin clone 84d, mouse antivinculin clone 4505, and mouse anti–α-actinin (Sigma-Aldrich); anti-PY clone 4G10 (Millipore); rabbit anti–Src-pY527 (Signal Transduction); mouse anti-Src (provided by J. Brugge, Harvard University, Cambridge, MA); rabbit antizyxin (provided by M. Beckerle, Huntsman Cancer Institute, Salt Lake City, UT); mouse anti–β-Pix (Millipore); and rabbit anti-GFP (Abcam). The following expression constructs were used: sources of EGFP conjugates of α-actinin, talin, paxillin, FAK, and zyxin were described previously (Hu et al., 2007). EGFP-paxillin was obtained from R. Horwitz (University of Virginia, Charlottesville, VA) and mApple-paxillin, EGFP vinculin, and mCherry vinculin were provided by M. Davidson (Florida State University, Tallahassee, FL). The EGFP conjugates of paxillin and paxillin mutants were based on the original sequence for avian paxillin-EGFP (Laukaitis et al., 2001) but were generated by synthesis (Blue Heron Biotechnology) and included mutations rendering dead an internal translation site of avian paxillin as described previously (Tumbarello et al., 2005; Schneider et al., 2009).

Western blot analysis

Whole cell extracts from MEF cells were prepared in lysis buffer containing 50 mM Tris, pH 8.0, 150 mM NaCl, 5 mM EDTA, 5% glycerol, 1% Triton X-100, 25 mM NaF, and 2 mM $NaVO_4$ supplemented with 1× protease inhibitor cocktail (Roche) and phosphatase inhibitor cocktails I and II (Sigma-Aldrich). Cells were freeze thawed twice in liquid nitrogen and clarified by centrifugation at 16,000 *g*. Proteins from supernatants were quantified by the Bradford method. 10 µg of proteins were mixed with an equal volume of 2× Laemmli sample buffer and separated by SDS-PAGE. After electrophoresis, proteins were electrotransferred to an immobilon-P membrane. For protein detection, membranes were blocked for 1 h at room temperature with 5% nonfat dry milk (wt/vol) or 3% BSA for tyrosine phosphorylation blots in TBS-T buffer (20 mM Tris, pH 7.6, 137 mM $NaCl_2$, and 0.1% Tween-20 [vol/vol]) and incubated overnight at 4°C with the indicated antibodies. After primary antibody incubation, blots were washed three times with TBS-T (10 min each) and incubated with appropriate HRP-conjugated or fluorescent-labeled secondary antibodies (1:5,000 and 1:20,000, respectively) for 1 h. Blots were washed three times with TBS-T. Protein bands were visualized using an ECL detection system (Millipore) or fluorescent-labeled antibodies and imaging on a gel imaging system (Odyssey; LI-COR Biosciences). For analysis of ECL, digital images of Western blot bands were quantified with MetaMorph software (MDS Analytical Technologies) after performing local background subtraction around bands of interest.

IPs

MEF cells were plated in 15-cm tissue culture plates precoated with 5 µg/ml fibronectin and supplemented with 10% FBS for 16 h. Cells were treated with myosin II inhibitors (20 µM blebbistatin) for 1 h. For EGFP-paxillin mutants, EGFP-positive cells were cell sorted and collected by flow cytometry and replated in dishes precoated with 5 µg/ml fibronectin after transfection. Cells were harvested in lysis buffer, clarified by centrifugation, and protein in supernatants was quantified by the Bradford assay. For IP, supernatants (1.0 mg total protein for untransfected cells and 500 µg for EGFP-transfected cells) were precleared with anti–mouse or anti–rabbit IgG IP beads (TrueBlot; eBioscience), preclearing beads were pelleted, and supernatants were incubated with 1 µg primary antibody and rotated overnight at 4°C. The following day, the solution was incubated with 30 µl protein A sepharose beads (TrueBlot) with rotation at 4° for 1 h. Beads were washed three times with lysis buffer and resuspended in 30 µl 2× Laemmli sample buffer. Samples were analyzed by Western blotting using the appropriate antibodies.

Polyacrylamide substrates

Flexible polyacrylamide substrates were generated as previously described (Pelham and Wang, 1997). In brief, 22-mm coverslips were activated by treatment with 50% 3-aminopropyltrimethyloxysilane and 0.5% glutaraldehyde, and each treatment was followed by extensive double-distilled H_2O washing. Activated coverslips were inverted on a freshly mixed solution of 0.04% bis/7.5% acrylamide to give an adhered gel with a stiffness of 1.0 kPa. 8 µl of acrylamide solution was sufficient to obtain a ∼15–20-µm-thick gel. Coverslips with attached gel substrates were washed in double-distilled H_2O and spun dry using a custom-made coverslip spinner. To bind fibronectin, gel substrates were activated by 2 mg/ml sulfo-SANPAH with two 8-min UV exposures one inch from two 10-W, 254-nm UV bulbs (UVP). Activated, gel-bound coverslips were coated with 5 µg/ml fibronectin (EMD) incubated for 2 h at 37°C and washed three times with PBS.

Immunofluorescence

Coverslips with bound cells were fixed/permeabilized for 1 min at 37°C in 0.01% Triton X-100, 0.25% paraformaldehyde (Electron Microscopy Science), and 1 mg/ml phalloidin in cytoskeleton buffer (CB; 10 mM MES, 3 mM $MgCl_2$, 138 mM KCl, and 2 mM EGTA) and fixed in 3% paraformaldehyde in CB for 20 min at 37°C. After fixation, cells were permeabilized with 0.25% Triton X-100 in CB. Free aldehydes were reacted with 0.1 M glycine for 5 min, and cells were washed three times for 10 min in TBS and blocked in blocking solution (2% BSA IgG free and protease free; Jackson ImmunoResearch Laboratories, Inc.) in TBS-T containing Alexa Fluor 488 phalloidin (1:400; Invitrogen) for at least 1 h. Coverslips were incubated with primary antibodies diluted in blocking solution overnight in a humid chamber at 4°C. After primary antibody incubation, cells were washed four times for 10 min in TBS-T and incubated with fluorophore-conjugated secondary antibodies (Jackson ImmunoResearch Laboratories, Inc.) diluted 1:250 in blocking solution for 1 h, washed again, and mounted on a slide in mounting media (Dako) and sealed with nail polish.

Microscopy and image analysis

Fixed and immunolabeled cells were imaged on an inverted microscope system (Eclipse TE-300; Nikon; Wittmann et al., 2003) with a cooled charge-coupled device (CCD; Orca II; Hamamatsu Photonics) using a 60× 1.4 NA Plan Apo PH objective lens (Nikon) for cells plated on glass or a 60× 1.2 NA Plan Apo violet-corrected objective lens (WI; Nikon) for cells plated on polyacrylamide substrates. Time-lapse imaging of cell migration was performed at 37°C on the same microscope using a 10× 0.5 NA PH Plan objective lens (Nikon) and 0.52 NA condenser (LWD; Nikon), and images were captured at 5-min intervals for 24 h. Dual-color time-lapse TIRF microscopy of EGFP and mCherry- or mApple-tagged proteins in living MEFs was performed at 37°C in DME without Phenol red and supplemented with 10% FBS, 25 mM Hepes, and 10 U/ml oxyrase using a 100× 1.49 NA Plan objective lens (Nikon; Shin et al., 2010) and an inverted microscope system (TE2000E2; Nikon) with an evanescent field depth of ∼150 nm.

Published March 22, 2010

For EGFP images, the 488-nm laser was used, and for mCherry or mApple, the 561-nm laser was used. Pairs of EGFP and mCherry or mApple images were captured in rapid succession at 10-s intervals using a CCD (HQ2; Hamamatsu Photonics) operated in the 14-bit readout mode. FRAP of EGFP-tagged FA proteins was performed using a 100× 1.49 NA Plan Apo objective lens on an inverted microscope system (TE2000E2). 488-nm and 561-nm illumination provided by a 20-mW argon laser and a 10-mW solid-state laser, respectively (CVI Melles Griot), was fiber optically coupled (Oz Optics) to a dual-port photostimulation epi-illuminator (Nikon), which centered and expanded the laser beams on the objective lens back aperture to form a diffraction-limited spot at the specimen plane. The position of the specimen was adjusted using a robotic stage (Applied Scientific Instruments) to center the spot onto a single fluorescent FA. An electronic shutter (Sutter Instrument Co.) was used to limit exposure of the specimen to the laser beam to the time needed for photobleaching. For imaging, mercury arc illumination coupled to the epi-illuminator was electronically shuttered (Sutter Instrument Co.) and filtered (Chroma Technology Corp.) to provide excitation specific for EGFP or mCherry. Images were acquired at 1–30-s intervals before and after photobleaching using an EM-CCD (512B; Photometrics) operated in the 14-bit mode using EM gain. Image frequency was adjusted depending on the fluorescence photobleaching recovery rate of the fluorescent-tagged adhesion protein being imaged.

To quantify cell migration rate, time-lapse microscopy was performed at 37°C using an inverted microscope (Eclipse TE-300). Phase-contrast images were acquired every 5 min using a 10× 0.25 NA Plan objective lens and a 0.52 NA condenser (LWD). Positions of the cell nuclei were manually tracked over time using MetaMorph software. Instantaneous cell velocities were calculated as the displacement (micrometers) between consecutive frames divided by the elapsed time. Area of individual adhesions was measured from manually thresholded images of immunolocalized paxillin or PY as described previously (Schneider et al., 2009). In brief, adhesion area was quantified by thresholding the paxillin or PY immunostaining image by eye to include only adhesion areas using MetaMorph software. The normalized fluorescence in adhesions was calculated by dividing the background-subtracted mean fluorescence in the adhesion area by the background-subtracted mean fluorescence in the cytosol.

FRAP experiments were analyzed as follows. The intensity recovery of the bleached region was extracted from the images, corrected for photobleaching, and analysis of FRAP curves was performed as described previously (Phair et al., 2004). In brief, to extract the characteristic recovery time for the assayed fluorescent-tagged proteins, normalized and photobleaching-corrected curves were fit to single exponential functions. In the vinculin FRAP experiments, a single exponential fit often systematically deviated from the data, overestimating the recovery for early time points. These curves were subsequently fit with double exponentials, and the long time constant was reported. We attribute the fast time scale, needed to fit the early time points (<10 s), to diffusion of the unbound protein (Wolfenson et al., 2009). If the fit parameters did not converge within 20% of the optimum value for the 95% confidence bounds, the fast time scale and the offset were constrained to their midpoint values and the fit was recomputed.

Analysis of the intensity of EGFP and mCherry- or mApple-tagged proteins in adhesions in TIRF images was performed as follows. The maximal area of a single adhesion in a time-lapse sequence was outlined, and the intensity in that region in both image channels was recorded for each image in the two series. The mean (or standard deviation) of the background for each channel was considered as the mean (or standard deviation) of the intensity in this region before the assembly of the adhesion. The intensity values in each series were corrected by mean background subtraction and normalization to the maximal intensity in the series. A significant rise in intensity, indicating the initiation of recruitment of the fluorescent-tagged protein in the region, was considered as the first image in the series in which the corrected intensity rose to greater than two times the standard deviation of the background. The difference between initiation times for the two image channels represents the lag time between the accumulation of paxillin and vinculin at adhesions.

The change in the level of different FA proteins in adhesions after blebbistatin treatment in double-labeled immunofluorescence images was quantified in the following manner. Images of immunolocalized paxillin or PY were median filtered with a three-pixel square kernel, background flattened with a 13-pixel square kernel, and binarized based on a manually selected threshold level that allowed all FAs to be included. The boundaries of thresholded areas were used to create regions around segmented adhesions. The regions were transferred from the paxillin (or PY) immunofluorescence image to the FA protein immunofluorescence image (talin 1, FAK, β1 integrin, zyxin, vinculin, α-actinin, pY397 FAK, pY118 paxillin, or pY31 paxillin) of the same cell. The mean intensity of the fluorescence in FAs was background subtracted and averaged over several cells. 95% confidence intervals were calculated for paxillin (or PY) and the FA proteins in control and blebbistatin-treated cells. The mean paxillin (or PY) or FA protein intensity of the adhesions in blebbistatin-treated cells was divided by the mean intensity of the same protein in adhesions in control cells to generate the fractional FA immunofluorescence signal change after blebbistatin treatment as reported in the figures. For vanadate treatment experiments, mean FA protein intensity in adhesions in the blebbistatin-treated cells was divided by the mean FA protein intensity in cells treated with both blebbistatin and vanadate. Statistical significance ($P < 0.02$) was measured by a two-tailed Student's *t* test between control and blebbistatin-treated cells. The metric that was tested for significance was the background-subtracted intensity of the FA component divided by the background-subtracted intensity of paxillin (or PY).

Online supplemental material

Fig. S1 shows that substrate compliance causes reduction of vinculin and FAK in adhesions and reduction of FAK phosphorylation. Fig. S2 shows FRAP analysis of EGFP-tagged adhesion proteins. Fig. S3 shows that myosin II–mediated vinculin recruitment to adhesions is cell type independent. Fig. S4 shows that β-Pix localization to adhesions is myosin II independent. Fig. S5 shows that pharmacological inhibition of FAK does not inhibit vinculin binding to paxillin or localization to adhesions. Video 1 shows time-lapse TIRF images of EGFP-paxillin and mCherry-vinculin in an adhesion forming and growing at the leading edge of a migrating MEF cell. Online supplemental material is available at http://www.jcb.org/cgi/content/full/jcb.200906012/DC1.

We thank Joan Brugge, Mike Davidson, and Mary Beckerle for reagents, the NHLBI Flow Cytometry Core Facility, William Shin, Sergei Plotnikov, and members of the Waterman laboratory. Experiments in Fig. 3 were first performed in conjunction with Michelle Knowles in the Physiology Course at the Marine Biological Laboratory (Woods Hole, MA).

This work was supported by NHLBI (C.M. Waterman and A.M. Pasapera; and grant HL093156 to D.D. Schlaepfer) and the Burroughs Wellcome Fund (E. Rericha).

Submitted: 2 June 2009
Accepted: 19 February 2010

References

Ballestrem, C., N. Erez, J. Kirchner, Z. Kam, A. Bershadsky, and B. Geiger. 2006. Molecular mapping of tyrosine-phosphorylated proteins in focal adhesions using fluorescence resonance energy transfer. *J. Cell Sci.* 119:866–875. doi:10.1242/jcs.02794

Bellis, S.L., J.T. Miller, and C.E. Turner. 1995. Characterization of tyrosine phosphorylation of paxillin in vitro by focal adhesion kinase. *J. Biol. Chem.* 270:17437–17441. doi:10.1074/jbc.270.29.17437

Bertolucci, C.M., C.D. Guibao, and J.J. Zheng. 2008. Phosphorylation of paxillin LD4 destabilizes helix formation and inhibits binding to focal adhesion kinase. *Biochemistry.* 47:548–554. doi:10.1021/bi702103n

Brown, M.C., J.A. Perrotta, and C.E. Turner. 1996. Identification of LIM3 as the principal determinant of paxillin focal adhesion localization and characterization of a novel motif on paxillin directing vinculin and focal adhesion kinase binding. *J. Cell Biol.* 135:1109–1123. doi:10.1083/jcb.135.4.1109

Bulinski, J.C., D.J. Odde, B.J. Howell, T.D. Salmon, and C.M. Waterman-Storer. 2001. Rapid dynamics of the microtubule binding of ensconsin in vivo. *J. Cell Sci.* 114:3885–3897.

Burridge, K., C.E. Turner, and L.H. Romer. 1992. Tyrosine phosphorylation of paxillin and pp125FAK accompanies cell adhesion to extracellular matrix: a role in cytoskeletal assembly. *J. Cell Biol.* 119:893–903. doi:10.1083/jcb.119.4.893

Cai, Y.F., N. Biais, G. Giannone, M. Tanase, G.Y. Jiang, J.M. Hofman, C.H. Wiggins, P. Silberzan, A. Buguin, B. Ladoux, and M.P. Sheetz. 2006. Nonmuscle myosin IIA-dependent force inhibits cell spreading and drives F-actin flow. *Biophys. J.* 91:3907–3920. doi:10.1529/biophysj.106.084806

Chandrasekar, I., T.E. Stradal, M.R. Holt, F. Entschladen, B.M. Jockusch, and W.H. Ziegler. 2005. Vinculin acts as a sensor in lipid regulation of adhesion-site turnover. *J. Cell Sci.* 118:1461–1472. doi:10.1242/jcs.01734

Chen, H., D.M. Choudhury, and S.W. Craig. 2006. Coincidence of actin filaments and talin is required to activate vinculin. *J. Biol. Chem.* 281:40389–40398. doi:10.1074/jbc.M607324200

Choi, C.K., M. Vicente-Manzanares, J. Zareno, L.A. Whitmore, A. Mogilner, and A.R. Horwitz. 2008. Actin and alpha-actinin orchestrate the assembly and maturation of nascent adhesions in a myosin II motor-independent manner. *Nat. Cell Biol.* 10:1039–1050. doi:10.1038/ncb1763

Chrzanowska-Wodnicka, M., and K. Burridge. 1996. Rho-stimulated contractility drives the formation of stress fibers and focal adhesions. *J. Cell Biol.* 133:1403–1415. doi:10.1083/jcb.133.6.1403

del Rio, A., R. Perez-Jimenez, R.C. Liu, P. Roca-Cusachs, J.M. Fernandez, and M.P. Sheetz. 2009. Stretching single talin rod molecules activates vinculin binding. *Science.* 323:638–641. doi:10.1126/science.1162912

Engler, A.J., S. Sen, H.L. Sweeney, and D.E. Discher. 2006. Matrix elasticity directs stem cell lineage specification. *Cell.* 126:677–689. doi:10.1016/j.cell.2006.06.044

Even-Ram, S., A.D. Doyle, M.A. Conti, K. Matsumoto, R.S. Adelstein, and K.M. Yamada. 2007. Myosin IIA regulates cell motility and actomyosin-microtubule crosstalk. *Nat. Cell Biol.* 9:299–309. doi:10.1038/ncb1540

Friedland, J.C., M.H. Lee, and D. Boettiger. 2009. Mechanically activated integrin switch controls alpha5beta1 function. *Science.* 323:642–644. doi:10.1126/science.1168441

Galbraith, C.G., K.M. Yamada, and M.P. Sheetz. 2002. The relationship between force and focal complex development. *J. Cell Biol.* 159:695–705. doi:10.1083/jcb.200204153

Geiger, B., J.P. Spatz, and A.D. Bershadsky. 2009. Environmental sensing through focal adhesions. *Nat. Rev. Mol. Cell Biol.* 10:21–33. doi:10.1038/nrm2593

Hagel, M., E.L. George, A. Kim, R. Tamimi, S.L. Opitz, C.E. Turner, A. Imamoto, and S.M. Thomas. 2002. The adaptor protein paxillin is essential for normal development in the mouse and is a critical transducer of fibronectin signaling. *Mol. Cell. Biol.* 22:901–915. doi:10.1128/MCB.22.3.901-915.2002

Hu, K., L. Ji, K.T. Applegate, G. Danuser, and C.M. Waterman-Storer. 2007. Differential transmission of actin motion within focal adhesions. *Science.* 315:111–115. doi:10.1126/science.1135085

Ilić, D., Y. Furuta, S. Kanazawa, N. Takeda, K. Sobue, N. Nakatsuji, S. Nomura, J. Fujimoto, M. Okada, and T. Yamamoto. 1995. Reduced cell motility and enhanced focal adhesion contact formation in cells from FAK-deficient mice. *Nature.* 377:539–544. doi:10.1038/377539a0

Jiang, G.Y., G. Giannone, D.R. Critchley, E. Fukumoto, and M.P. Sheetz. 2003. Two-piconewton slip bond between fibronectin and the cytoskeleton depends on talin. *Nature.* 424:334–337. doi:10.1038/nature01805

Jones, P., P. Jackson, G.J. Price, B. Patel, V. Ohanion, A.L. Lear, and D.R. Critchley. 1989. Identification of a talin binding site in the cytoskeletal protein vinculin. *J. Cell Biol.* 109:2917–2927. doi:10.1083/jcb.109.6.2917

Kmiecik, T.E., and D. Shalloway. 1987. Activation and suppression of pp60c-src transforming ability by mutation of its primary sites of tyrosine phosphorylation. *Cell.* 49:65–73. doi:10.1016/0092-8674(87)90756-2

Laukaitis, C.M., D.J. Webb, K. Donais, and A.F. Horwitz. 2001. Differential dynamics of α 5 integrin, paxillin, and α-actinin during formation and disassembly of adhesions in migrating cells. *J. Cell Biol.* 153:1427–1440. doi:10.1083/jcb.153.7.1427

Lee, H.S., R.M. Bellin, D.L. Walker, B. Patel, P. Powers, H.J. Liu, B. Garcia-Alvarez, J.M. de Pereda, R.C. Liddington, N. Volkmann, et al. 2004. Characterization of an actin-binding site within the talin FERM domain. *J. Mol. Biol.* 343:771–784. doi:10.1016/j.jmb.2004.08.069

Lele, T.P., and D.E. Ingber. 2006. A mathematical model to determine molecular kinetic rate constants under non-steady state conditions using fluorescence recovery after photobleaching (FRAP). *Biophys. Chem.* 120:32–35. doi:10.1016/j.bpc.2005.10.007

Möhl, C., N. Kirchgessner, C. Schäfer, K. Küpper, S. Born, G. Diez, W.H. Goldmann, R. Merkel, and B. Hoffmann. 2009. Becoming stable and strong: the interplay between vinculin exchange dynamics and adhesion strength during adhesion site maturation. *Cell Motil. Cytoskeleton.* 66:350–364. doi:10.1002/cm.20375

Nayal, A., D.J. Webb, C.M. Brown, E.M. Schaefer, M. Vicente-Manzanares, and A.R. Horwitz. 2006. Paxillin phosphorylation at Ser273 localizes a GIT1-PIX-PAK complex and regulates adhesion and protrusion dynamics. *J. Cell Biol.* 173:587–589. doi:10.1083/jcb.200509075

Opazo Saez, A., W. Zhang, Y. Wu, C.E. Turner, D.D. Tang, and S.J. Gunst. 2004. Tension development during contractile stimulation of smooth muscle requires recruitment of paxillin and vinculin to the membrane. *Am. J. Physiol. Cell Physiol.* 286:C433–C447. doi:10.1152/ajpcell.00030.2003

Pelham, R.J. Jr., and Y.L. Wang. 1997. Cell locomotion and focal adhesions are regulated by substrate flexibility. *Proc. Natl. Acad. Sci. USA.* 94:13661–13665. doi:10.1073/pnas.94.25.13661

Petit, V., B. Boyer, D. Lentz, C.E. Turner, J.P. Thiery, and A.M. Vallés. 2000. Phosphorylation of tyrosine residues 31 and 118 on paxillin regulates cell migration through an association with CRK in NBT-II cells. *J. Cell Biol.* 148:957–970. doi:10.1083/jcb.148.5.957

Phair, R.D., S.A. Gorski, and T. Misteli. 2004. Measurement of dynamic protein binding to chromatin in vivo, using photobleaching microscopy. *Methods Enzymol.* 375:393–414. doi:10.1016/S0076-6879(03)75025-3

Riveline, D., E. Zamir, N.Q. Balaban, U.S. Schwarz, T. Ishizaki, S. Narumiya, Z. Kam, B. Geiger, and A.D. Bershadsky. 2001. Focal contacts as mechanosensors: externally applied local mechanical force induces growth of focal contacts by an mDia1-dependent and ROCK-independent mechanism. *J. Cell Biol.* 153:1175–1186. doi:10.1083/jcb.153.6.1175

Roberts, W.G., E. Ung, P. Whalen, B. Cooper, C. Hulford, C. Autry, D. Richter, E. Emerson, J. Lin, J. Kath, et al. 2008. Antitumor activity and pharmacology of a selective focal adhesion kinase inhibitor, PF-562,271. *Cancer Res.* 68:1935–1944. doi:10.1158/0008-5472.CAN-07-5155

Sawada, Y., M. Tamada, B.J. Dubin-Thaler, O. Cherniavskaya, R. Sakai, S. Tanaka, and M.P. Sheetz. 2006. Force sensing by mechanical extension of the Src family kinase substrate p130Cas. *Cell.* 127:1015–1026. doi:10.1016/j.cell.2006.09.044

Schaller, M.D., and J.T. Parsons. 1995. pp125FAK-dependent tyrosine phosphorylation of paxillin creates a high-affinity binding site for Crk. *Mol. Cell. Biol.* 15:2635–2645.

Schaub, S., S. Bohnet, V.M. Laurent, J.J. Meister, and A.B. Verkhovsky. 2007. Comparative maps of motion and assembly of filamentous actin and myosin II in migrating cells. *Mol. Biol. Cell.* 18:3723–3732. doi:10.1091/mbc.E06-09-0859

Schlaepfer, D.D., and T. Hunter. 1996. Evidence for in vivo phosphorylation of the Grb2 SH2-domain binding site on focal adhesion kinase by Src-family protein-tyrosine kinases. *Mol. Cell. Biol.* 16:5623–5633.

Schmalzigaug, R., M.L. Garron, J.T. Roseman, Y. Xing, C.E. Davidson, S.T. Arold, and R.T. Premont. 2007. GIT1 utilizes a focal adhesion targeting-homology domain to bind paxillin. *Cell. Signal.* 19:1733–1744. doi:10.1016/j.cellsig.2007.03.010

Schneider, I.C., C.K. Hays, and C.M. Waterman. 2009. Epidermal growth factor-induced contraction regulates paxillin phosphorylation to temporally separate traction generation from de-adhesion. *Mol. Biol. Cell.* 20:3155–3167. doi:10.1091/mbc.E09-03-0219

Shi, Q., and D. Boettiger. 2003. A novel mode for integrin-mediated signaling: tethering is required for phosphorylation of FAK Y397. *Mol. Biol. Cell.* 14:4306–4315. doi:10.1091/mbc.E03-01-0046

Shin, W., R.S. Fischer, P. Kanchanawong, Y. Kim, J. Lim, K.A. Meyers, Y. Nishimura, S.V. Plotnikov, I. Thievessen, D. Yarar, et al. 2010. A versatile, multi-color total internal reflection fluorescence and spinning disk confocal microscope system for high-resolution live cell imaging. *In* Live Cell Imaging. A Laboratory Manual. R.D. Goldman, J. Swedlow, and D.L. Spector, editors. Cold Spring Harbor Laboratory Press, Cold Spring Harbor, NY. 119–138.

Tadokoro, S., S.J. Shattil, K. Eto, V. Tai, R.C. Liddington, J.M. de Pereda, M.H. Ginsberg, and D.A. Calderwood. 2003. Talin binding to integrin beta tails: a final common step in integrin activation. *Science.* 302:103–106. doi:10.1126/science.1086652

Thomas, S.M., and J.S. Brugge. 1997. Cellular functions regulated by Src family kinases. *Annu. Rev. Cell Dev. Biol.* 13:513–609. doi:10.1146/annurev.cellbio.13.1.513

Thomas, S.M., M. Hagel, and C.E. Turner. 1999. Characterization of a focal adhesion protein, Hic-5, that shares extensive homology with paxillin. *J. Cell Sci.* 112:181–190.

Torsoni, A.S., T.M. Marin, L.A. Velloso, and K.G. Franchini. 2005. RhoA/ROCK signaling is critical to FAK activation by cyclic stretch in cardiac myocytes. *Am. J. Physiol. Heart Circ. Physiol.* 289:H1488–H1496. doi:10.1152/ajpheart.00692.2004

Totsukawa, G., Y. Wu, Y. Sasaki, D.J. Hartshorne, Y. Yamakita, S. Yamashiro, and F. Matsumura. 2004. Distinct roles of MLCK and ROCK in the regulation of membrane protrusions and focal adhesion dynamics during cell migration of fibroblasts. *J. Cell Biol.* 164:427–439. doi:10.1083/jcb.200306172

Tumbarello, D.A., M.C. Brown, S.E. Hetey, and C.E. Turner. 2005. Regulation of paxillin family members during epithelial-mesenchymal transformation: a putative role for paxillin delta. *J. Cell Sci.* 118:4849–4863. doi:10.1242/jcs.02615

Turner, C.E. 2000. Paxillin interactions. *J. Cell Sci.* 113:4139–4140.

Turner, C.E., M.C. Brown, J.A. Perrotta, M.C. Riedy, S.N. Nikolopoulos, A.R. McDonald, S. Bagrodia, S. Thomas, and P.S. Leventhal. 1999. Paxillin LD4 motif binds PAK and PIX through a novel 95-kD ankyrin repeat, ARF-GAP protein: A role in cytoskeletal remodeling. *J. Cell Biol.* 145:851–863. doi:10.1083/jcb.145.4.851

Vogel, V., and M. Sheetz. 2006. Local force and geometry sensing regulate cell functions. *Nat. Rev. Mol. Cell Biol.* 7:265–275. doi:10.1038/nrm1890

Webb, D.J., K. Donais, L.A. Whitmore, S.M. Thomas, C.E. Turner, J.T. Parsons, and A.F. Horwitz. 2004. FAK-Src signalling through paxillin, ERK

and MLCK regulates adhesion disassembly. *Nat. Cell Biol.* 6:154–161. doi:10.1038/ncb1094

Wiseman, P.W., C.M. Brown, D.J. Webb, B. Hebert, N.L. Johnson, J.A. Squier, M.H. Ellisman, and A.F. Horwitz. 2004. Spatial mapping of integrin interactions and dynamics during cell migration by image correlation microscopy. *J. Cell Sci.* 117:5521–5534. doi:10.1242/jcs.01416

Wittmann, T., G.M. Bokoch, and C.M. Waterman-Storer. 2003. Regulation of leading edge microtubule and actin dynamics downstream of Rac1. *J. Cell Biol.* 161:845–851. doi:10.1083/jcb.200303082

Wolfenson, H., A. Lubelski, T. Regev, J. Klafter, Y.I. Henis, and B. Geiger. 2009. A role for the juxtamembrane cytoplasm in the molecular dynamics of focal adhesions. *PLoS One.* 4:e4304. doi:10.1371/journal.pone.0004304

Zaidel-Bar, R., C. Ballestrem, Z. Kam, and B. Geiger. 2003. Early molecular events in the assembly of matrix adhesions at the leading edge of migrating cells. *J. Cell Sci.* 116:4605–4613. doi:10.1242/jcs.00792

Zaidel-Bar, R., M. Cohen, L. Addadi, and B. Geiger. 2004. Hierarchical assembly of cell-matrix adhesion complexes. *Biochem. Soc. Trans.* 32:416–420. doi:10.1042/BST0320416

Zaidel-Bar, R., S. Itzkovitz, A. Ma'ayan, R. Iyengar, and B. Geiger. 2007a. Functional atlas of the integrin adhesome. *Nat. Cell Biol.* 9:858–867. doi:10.1038/ncb0807-858

Zaidel-Bar, R., R. Milo, Z. Kam, and B. Geiger. 2007b. A paxillin tyrosine phosphorylation switch regulates the assembly and form of cell-matrix adhesions. *J. Cell Sci.* 120:137–148. doi:10.1242/jcs.03314

Zhang, X., G. Jiang, Y. Cai, S.J. Monkley, D.R. Critchley, and M.P. Sheetz. 2008. Talin depletion reveals independence of initial cell spreading from integrin activation and traction. *Nat. Cell Biol.* 10:1062–1068. doi:10.1038/ncb1765

Zhu, J.H., B.H. Luo, T. Xiao, C.Z. Zhang, N. Nishida, and T.A. Springer. 2008. Structure of a complete integrin ectodomain in a physiologic resting state and activation and deactivation by applied forces. *Mol. Cell.* 32:849–861. doi:10.1016/j.molcel.2008.11.018

Zimerman, B., T. Volberg, and B. Geiger. 2004. Early molecular events in the assembly of the focal adhesion-stress fiber complex during fibroblast spreading. *Cell Motil. Cytoskeleton.* 58:143–159. doi:10.1002/cm.20005